Consistent with low modelled reactive chlorine concentrations, several workers report model underpredictions of ozone depletion of between 25 and 40% (refs 16, 17), although these discrepancies may be due partly to incorrectly modelled gas-phase reactions rather than heterogeneous processing. Edouard *et al.*[22] have suggested that such underprediction by three-dimensional models may be caused by averaging small-scale structure in species concentration over large grid boxes. This arises because of the nonlinear dependence of key reaction rates on concentration. This offers a possible explanation for underpredicted ozone loss in three-dimensional models, but does not explain low modelled ClO and does not refer to predictions of trajectory models[13]. Whether uncertainties in the temperature fields used in models are responsible for model underpredictions[13,15], or whether the mountain-wave activation mechanism suggested here is inappropriate can only be assessed by undertaking a multi-year model simulation and comparison with available data. However, it should be noted that mountain waves can act as a continuous source of inhomogeneities in reactive chlorine concentrations on a scale of a few kilometres, which, according to the findings of Edouard *et al.*[22], will make their inclusion in three-dimensional models highly problematic.

Other sources of gravity waves should also be examined for their potential role in chlorine activation; Wu and Waters[23,24] have shown from satellite data that there is evidence for middle-atmosphere gravity waves that correlate not only with surface topography but also with upper-tropospheric convection and stratospheric polar vortices. Gravity waves occurring at the vortex edge should also be examined for their potential contribution to the general decrease in ozone which has been observed at middle latitudes over the past decade[1]. □

Received 30 July 1997; accepted 8 January 1998.

1. *Scientific Assessment of Ozone Depletion: 1994* (Rep. No. 37, World Meteorological Organisation, Geneva, 1994).
2. Jones, R. L., McKenna, D. S., Poole, L. R. & Solomon, S. On the influence of polar stratospheric cloud formation on chemical composition during the 1988/89 Arctic winter. *Geophys. Res. Lett.* **17,** 545–548 (1990).
3. McKenna, D.S. *et al*. Calculations of ozone destruction during the 1988/89 Arctic winter. *Geophys. Res. Lett.* **17,** 553–556 (1990).
4. Borrmann, S. *et al*. Heterogeneous reactions on stratospheric background aerosols, volcanic sulfuric acid droplets, and type I polar stratospheric clouds. *J. Geophys. Res.* **102,** 3639–3648 (1997).
5. Gary, B. L. Observational results using the microwave temperature profiler during the Airborne Antarctic Ozone Experiment. *J. Geophys. Res.* **94,** 11223–11231 (1989).
6. Volkert, H. & Intes, D. Orographically forced stratospheric waves over northern Scandinavia. *Geophys. Res. Lett.* **19,** 1205–1208 (1992).
7. Leutbecher, M. & Volkert, H. Stratospheric temperature anomalies and mountain waves: A three dimensional simulation using a multi-scale weather prediction model. *Geophys. Res. Lett.* **23,** 3329–3332 (1996).
8. Bacmeister, J. T., Newman, P. A., Gary, B. L. & Chan, K. R. An algorithm for forecasting mountain wave-related turbulence in the stratosphere. *Weath. Forecst.* **9,** 241–253 (1994).
9. Dörnbrack, A., Leutbecher, M., Volkert, H. & Wirth, M. Mesoscale forecasts of stratospheric mountain waves. *Meteorol. Applic.* (in the press).
10. Stanford, J. L. & Davis, J. S. A century of stratospheric cloud reports: 1870–1972. *Bull. Am. Meteorol. Soc.* **55,** 213–219 (1974).
11. Peter, Th., Müller, R., Drdla, K., Petzoldt, K. & Reimer, E. A microphysical box model for EASOE: Preliminary results for the January/February 1990 PSC event over Kiruna. *Ber. Bunsenges. Phys. Chem.* **96,** 362–367 (1992).
12. Carslaw, K. S. *et al*. Particle microphysics and chemistry in remotely observed mountain polar stratospheric clouds. *J. Geophys. Res.* (in the press).
13. Lutman, E. R. *et al*. Three-dimensional studies of the 1991/92 northern hemisphere winter using domain-filling trajectories with chemistry. *J. Geophys. Res.* **102,** 1479–1488 (1997).
14. Bell, W. *et al*. Measurements of stratospheric chlorine monoxide (ClO) from ground-based FTIR observations. *J. Atmos. Chem.* **24,** 285–297 (1996).
15. Douglass, A. *et al*. A three-dimensional simulation of the early winter distribution of reactive chlorine in the north polar vortex. *Geophys. Res. Lett.* **20,** 1271–1274 (1993).
16. Goutail, F. *et al*. in *Polar Stratospheric Ozone* (eds Pyle, J. A., Harris, N. P. & Amanatidis, G. T.) 574–579 (Air Pollution Res. Rep. No. 56, European Communities, Brussels, 1996).
17. Hansen, G., Svenøe, T., Chipperfield, M. P., Dahlback, A. & Hoppe, U.-P. Evidence of substantial ozone depletion in winter 1995/96 over northern Norway. *Geophys. Res. Lett.* **24,** 799–802 (1997).
18. Carslaw, K. S., Peter, Th. & Clegg, S. L. Modeling the composition of liquid stratospheric aerosols. *Revs. Geophys.* **35,** 125–154 (1997).
19. Knudsen, B. M. Accuracy of Arctic stratospheric temperature analyses and the implications for the prediction of polar stratospheric clouds. *Geophys. Res. Lett.* **23,** 3747–3750 (1996).
20. Mishchenko, M. I. Light scattering by randomly oriented axially symmetric particles. *J. Opt. Soc. Am.* **8,** 871–882 (1991).
21. DeMore, W. *et al*. *Chemical Kinetics and Photochemical Data for Use in Stratospheric Modeling* (Publ. 97-4, Jet Propulsion Lab., Pasadena, 1997).
22. Edouard, S., Legras, B., Lefevre, F. & Eymard, R. The effect of small-scale inhomogeneities on ozone depletion in the Arctic. *Nature* **384,** 444–447 (1996).
23. Wu, D. L. & Waters, J. W. Gravity-wave-scale temperature fluctuations seen by the UARS MLS. *Geophys. Res. Lett.* **23,** 3289–3292 (1996).
24. Wu, D. L. & Waters, J. W. Satellite observations of atmospheric variances—a possible indication of gravity waves. *Geophys. Res. Lett.* **24,** 3631–3634 (1996).
25. Meilinger, S. K. *et al*. Size-dependent stratospheric droplet composition in lee wave temperature fluctuations and their potential role in PSC freezing. *Geophys. Res. Lett.* **22,** 3031–3034 (1995).
26. Müller, R. *et al*. Chlorine chemistry and the potential for ozone depletion in the Arctic stratosphere in the winter 1991/92. *Geophys. Res. Lett.* **21,** 1427–1430 (1994).
27. Carslaw, K. S., Peter, Th. & Müller, R. Uncertainties in reactive uptake coefficients for solid stratospheric particles—2. Effect on ozone depletion. *Geophys. Res. Lett.* **24,** 1747–1750 (1997).

Acknowledgements. We thank M. Mishchenko for help with the T-matrix calculations. Part of this work was funded by the European Communities, the German BMBF, the Office of Naval Research (ONR) and NASA's Atmospheric Chemistry Modeling and Analysis Program (ACMAP).

Correspondence and requests for materials should be sent to K.S.C. (e-mail: carslaw@mpch-mainz.mpg.de).

Reduced sensitivity of recent tree-growth to temperature at high northern latitudes

K. R. Briffa*, F. H. Schweingruber†, P. D. Jones*, T. J. Osborn*, S. G. Shiyatov‡ & E. A. Vaganov§

* *Climatic Research Unit, University of East Anglia, Norwich NR4 7TJ, UK*
† *Swiss Federal Institute of Forest, Snow and Landscape Research, Zürcherstrasse 111, CH-8903, Birmensdorf, Switzerland*
‡ *Institute of Plant and Animal Ecology, Ural Branch of the Russian Academy of Sciences, 8 Marta Street, Ekaterinburg 620219, Russia*
§ *Institute of Forest, Siberian Branch of the Russian Academy of Sciences, Krasnoyarsk, Russia*

Tree-ring chronologies that represent annual changes in the density of wood formed during the late summer can provide a proxy for local summertime air temperature[1]. Here we undertake an examination of large-regional-scale wood-density/air-temperature relationships using measurements from hundreds of sites at high latitudes in the Northern Hemisphere. When averaged over large areas of northern America and Eurasia, tree-ring density series display a strong coherence with summer temperature measurements averaged over the same areas, demonstrating the ability of this proxy to portray mean temperature changes over sub-continents and even the whole Northern Hemisphere. During the second half of the twentieth century, the decadal-scale trends in wood density and summer temperatures have increasingly diverged as wood density has progressively fallen. The cause of this increasing insensitivity of wood density to temperature changes is not known, but if it is not taken into account in dendroclimatic reconstructions, past temperatures could be overestimated. Moreover, the recent reduction in the response of trees to air-temperature changes would mean that estimates of future atmospheric CO_2 concentrations, based on carbon-cycle models that are uniformly sensitive to high-latitude warming, could be too low.

We have based this analysis on tree-growth data derived from trees sampled at more than 300 locations spread across the Northern Hemisphere (Fig. 1). These generally cool and moist sites were all chosen at relatively high latitudes or high elevations for the potential sensitivity of year-by-year tree growth to local temperature variability[2]. Though many of the sites are not strictly at tree-line, these data are a good proxy for the growth of the northern part of the boreal forest, rather than the large areas of closed-canopy, more drought-sensitive southern coniferous forests. Ring widths and the densities of the parts of the rings formed in late summer (maximum-latewood ring densities) were measured using multiple tree cores from each site[1]. The measurement series were then individually detrended to remove inherent age-related bias, by taking residuals from a simple function fit to the raw data and the resulting dimensionless indices averaged to form separate ring-width and

density chronologies for each site[3]. The detrending process results in a loss of multi-century variance, the extent of which is dependent on tree age and the flexibility of the fitted function[4,5]. These chronologies represent tree growth variability on timescales of years to centuries.

The fidelity of the local temperature sensitivity of these data has been clearly demonstrated by comparison with instrumental records and by the use of similar chronologies, or groups of chronologies, to reconstruct either regional-mean or detailed spatial patterns of past temperature variability at various locations, such as in northern Fennoscandia, western and northern North America and northern Russia[2,6–9], frequently using principal component regression techniques[10]. Here we have simply combined the dimensionless chronologies into large regional mean series, as defined in Fig. 1 legend, and rescaled the regional means and variances to match over a common base (1881–1940). Our purpose is to identify very large (sub-continental scale) growth signals, necessarily obscuring any individual and localized site factors.

Table 1a shows the strength of the associations between these regional chronologies and summer mean temperatures[11] (April–September for density and June–August for the ring-width comparisons) averaged over similar areas (Fig. 1). The correlations focus separately on short (interannual) and longer-timescale (decadal and above) common variability in that they are calculated using high-pass (<10-year) and low-pass (>10-year) filtered data respectively.

On the interannual timescale, averaged across all regions, about

Table 1 Correlations between tree-ring and temperature series

	Maximum-latewood density*				Ring widths†			
	Interannual‡		Decadal§		Interannual		Decadal	
	1881–1960	1881–1981	1881–1960	1881–1981	1881–1960	1881–1981	1881–1960	1881–1981
a Regional-mean tree-growth series versus temperature								
NWNA‖	71	66	58	46	35	33	12	15
SWNA	72	75	72	63	27	22	–4	4
ENA	72	73	82	70	33	31	26	15
NEUR	89	87	92	81	73	64	56	45
SEUR	59	62	82	79	44	39	–6	7
WSIB	82	83	75	58	41	42	45	28
CSIB	56	51	83	67	42	34	54	44
ESIB	52	56	78	52	27	37	21	37
NORTH	73	71	90	60	32	28	78	34
SOUTH	64	67	73	65	37	41	12	13
ALL	68	70	89	64	47	47	74	43
b Tree-growth series versus Northern Hemisphere mean temperatures								
NORTH	45	44	74	41	16	11	79	42
SOUTH	2	10	61	40	8	14	25	28
ALL	33	36	81	46	19	17	75	51

All correlations in this table have been multiplied by 100.
* Correlated against April–September mean instrumental averages.
† Correlated against June–August instrumental data.
‡ Interannual correlations involve timeseries of residuals from decadally smoothed curves.
§ Decadal correlations are calculated using decadally smoothed series.
‖ Regional acronyms defined in Fig. 1 legend.

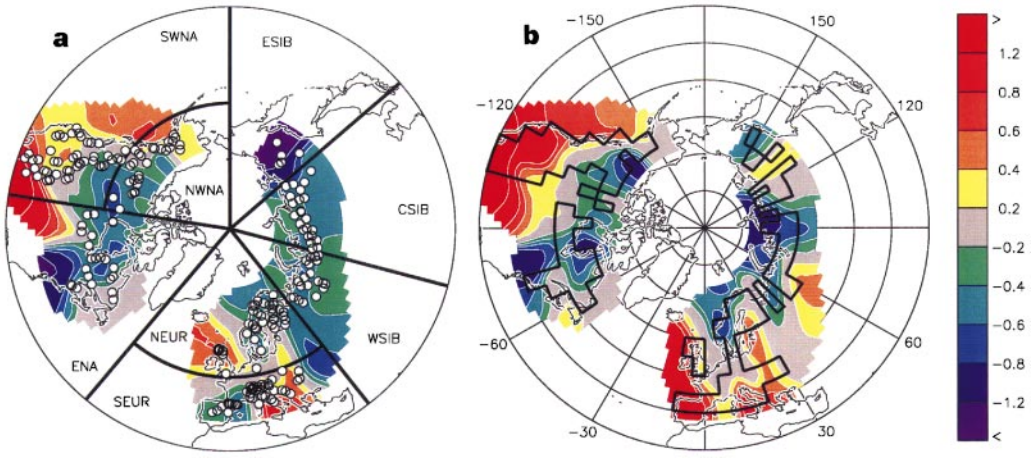

Figure 1 Spatial patterns of relative tree-growth decline. **a**, The location (circles) of tree-ring chronologies and the division (black lines) into regional averages. **b**, The locations (black lines) of the grid-box temperatures used for comparison with the tree growth series. The coloured contours show where the ring density (**a**) and ring width (**b**) are enhanced (positive) or suppressed (negative) relative to summer temperature during the period 1975–85 compared to the period 1935–45. Values are dimensionless, being the change in the difference of two normalized time series in each grid box. Definition of regions and number of sites: southwestern (SWNA, 53 sites), northwestern (NWNA, 30) and eastern (ENA, 34) North America; northern (NEUR, 46) and southern (SEUR, 72) Europe; western (WSIB, 42), central (CSIB, 31) and eastern (ESIB, 6) Siberia; all 125 sites in SWNA and SEUR form the composite region SOUTH, and all 189 sites in the six northern regions form the NORTH region; ALL is an average of all 314 sites.

50% of the variance (r^2) of each temperature series is common to the density series, with the individual regional variances ranging from 80% (NEUR) to ~30% (CSIB and ESIB). Consistently similar correlations are achieved, either calculated over the shorter (1881–1960) or extended (to 1981) periods, or when larger regional density chronologies made up of the NORTH (incorporating the NWNA, ENA, NEUR, WSI, CSIB and ESIB) and SOUTH (SWNA and SEUR) data are compared with the equivalent regionally-averaged temperatures.

The regional correlations for the decadally smoothed densities and temperatures are, in general, higher than the interannual values, with per cent common variances ranging from 34 (NWNA) to 85 (NEUR) and averaging ~60%: but only for the period 1881–1960. When the decadal correlations are calculated over the longer 1881–1981 period, consistent falls in the common variances are apparent in all areas. The falls are relatively small in the southern regions (from 67% to 62% in SEUR; and from 52% to 40% in SWNA) but much greater in the northern areas with a maximum fall in ESIB of >30% (from 61% to 27%). The average degradation in decadal-timescale common variance is nearly 20% across all eight regions. This low-frequency loss in temperature sensitivity is even more apparent when the correlations for the larger regions are compared over the two periods: over 30% loss of common variance overall, with the simple correlations falling from 0.90 to 0.60 in the NORTH and from 0.73 to 0.65 in the SOUTH, and 0.89 to 0.64 in ALL (the average series for all 314 sites).

For the period before 1960, these smoothed NORTH and SOUTH density averages also have 55% and 37% variance in common, respectively, with the full 'Northern Hemisphere' (land and marine) mean temperature record[11] (NHT), while density series ALL has 66% variance in common with the NHT (Table 1b). (The latter can be compared with a value of 87% for the comparison between the actual temperature data for the 'ALL' region and the NHT series). Recalculating these density and NHT correlations over a period extended by only 21 years results in common variances falling by 17% and 16% for the NORTH and SOUTH series, and 21% for the ALL.

In general, the ring-width/temperature correlations are lower than those for the densities. This is particularly evident on an interannual timescale because ring widths are more strongly auto-correlated and may integrate temperature forcing over a wider, seasonal (perhaps annual) window and over more than a single year[9,12,13]. However, the recent relative loss of decadal temperature sensitivity is also apparent in the ring-width data and is more noticeable in the larger spatial aggregate series where the temperature associations are stronger, especially, as with density, in the northern regions.

Figure 2 illustrates the temporal changes in the association between the smoothed tree growth and appropriate temperature series for the eight individual regions and for the NORTH, SOUTH and ALL aggregate series. Instrumental summer temperatures show slight increases in all areas. Most of this warming occurred in the first half of this century so that mean temperature levels in recent decades and the warmth of the late 1980s only match, or barely exceed, the levels of earlier warm periods. A negative bias in the comparable tree-growth records during the second half of this century is apparent in all regions. In all but the two southern regions, the temperature and tree growth curves increasingly diverge. In the areas where the growth data extend through to the warm late 1980s and early 1990s (NEUR, WSIB, CSIB, ESIB), the divergence is at a maximum in the most recent years.

Averaged around the Northern Hemisphere, early tree growth

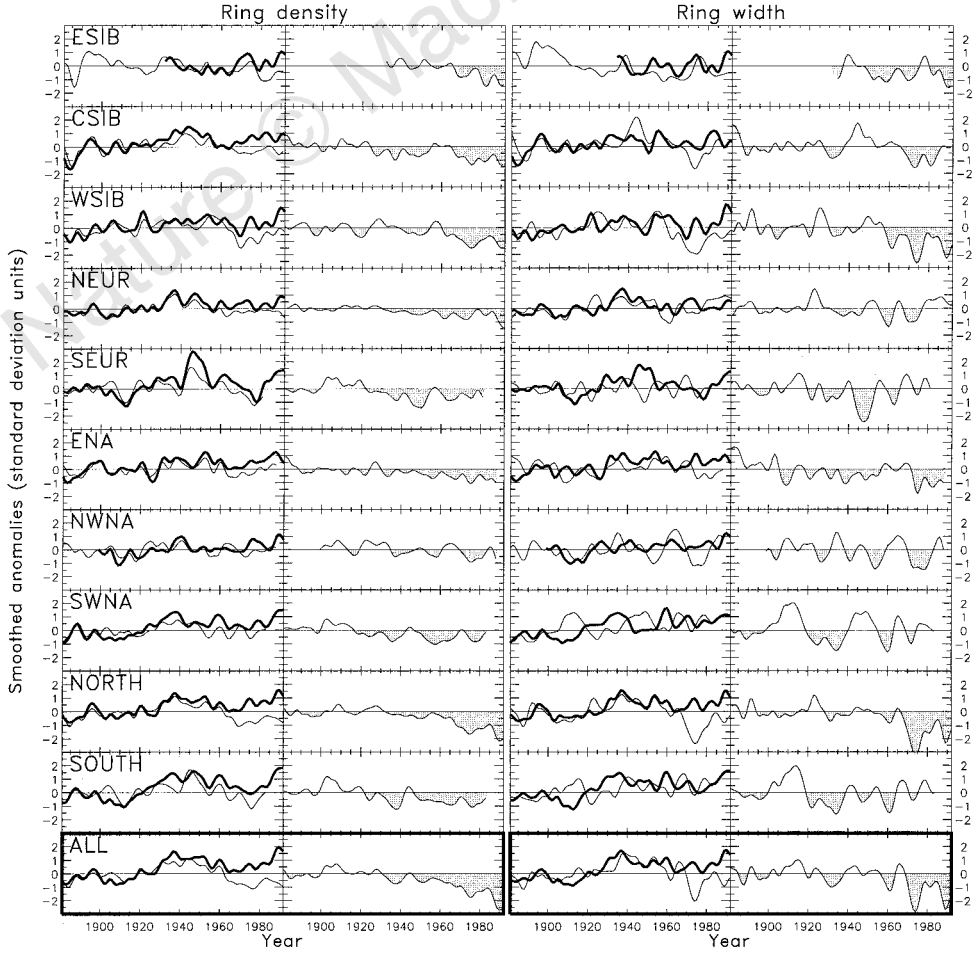

Figure 2 Regional tree growth and temperatures over the past 120 years. Decadally smoothed tree growth (thin lines), maximum-latewood density or ring width, plotted against mean summer temperatures (thick lines), April–September for density and June–August for ring width, for each of the regions described in Fig. 1. The difference series (growth minus temperature), shaded to emphasize negative values, are shown to the right of each pair of curves. All data series have been scaled to have zero mean and unit variance over the period 1881–1940 (except the short ESIB temperature series which uses 1932–75).

(ALL) can be seen to follow closely the decadal trends in recorded summer temperatures, tracking the rise to the relatively high levels of the 1930s and 1940s and the subsequent fall in the 1950s. However, although temperatures rose again after the mid-1960s and reached unprecedentedly high recorded levels by the late 1980s, hemispheric tree growth fell consistently after 1940, and in the late 1970s and 1980s reached levels as low as those attained in the cool 1880s. Over the hemisphere, the divergence between tree growth and mean summer temperatures began perhaps as early as the 1930s; became clearly recognisable, particularly in the north, after 1960; and has continued to increase up until the end of the common record at around 1990. The reason for this increasingly apparent and widespread phenomenon is not known but any one, or a combination, of several factors might be involved.

The positive linear thermal response of the trees may break down above some absolute threshold, perhaps with lower soil moisture exerting increasing stress at a number of sites[13]. However, the fidelity of the long-term growth response to the relatively high temperatures in the middle part of the century would imply the need for a concomitant lowering of soil moisture levels over very widespread areas during recent decades. There is little evidence that this has occurred in the regions represented by these trees[14,15]. Also the maintenance of high positive interannual temperature correlations during recent decades, argues against a simple soil-moisture-related explanation of the reducing tree growth. However, more subtle changes in precipitation or temperature seasonality, such as the documented move to warmer springs, and associated earlier snow melt[16] mean that it would be unwise to dismiss summer drought sensitivity too readily. Other factors such as increasing competition with other plants and increasing insect herbivory could play a role[17,18], but the apparent widespread synchroneity of the phenomenon suggests a hemispheric-scale influence. Higher UV-B levels[19–21] or decreased solar radiation receipts (increased optical depth)[22–24] may be involved, but attempting to isolate such effects will be problematic in the presence of increasing atmospheric CO_2 concentrations and increasing amounts of acidic deposition and tropospheric ozone, all of which, along with climate variability, are likely to influence tree growth[25,26].

Whatever the cause, this change in tree-growth response has important implications for studies of past and future climate change. The common use of least-squares regression for developing dendroclimatic transfer function equations to estimate past climates, imposes an equality of means in both the predictand and predictor time series over the fitting or 'calibration' period[10]. Any bias in mean tree growth will, therefore, be 'corrected' during calibration, with the consequence that the derived regression coefficients will be biased. Our results imply that this might increasingly result in systematic overestimation of past temperatures, particularly in regions where the loss of low-frequency temperature sensitivity in tree growth is greatest (eastern Siberia and eastern North America: see Fig. 1), where tree-ring 'standardization' is designed to preserve maximum long-timescale chronology variability[4], and where transfer functions are calibrated over the most recent decades.

The potential importance of these results for modelling future temperatures derives from their relevance to carbon-cycle-model experiments that seek to explain the history of measured atmospheric CO_2 concentrations and provide realistic projections[27,28]. Along with spatio-temporal analyses of past CO_2 measurements, these experiments show the existence of an important missing CO_2 sink, a large part of which is believed to be the northern terrestrial biosphere, including the boreal forest[29]. Accurate parametrization of the magnitude of this sink is necessary in order to reduce the uncertainties in the CO_2 mass balance and hence in projections of future CO_2 concentrations and climate[27]. Although we emphasize that our results apply generally only to the high-latitude temperature-sensitive forest regions of the Northern Hemisphere, the degradation in thermal response of this significant area of the world's biosphere suggests that we should be cautious in assuming, in carbon-cycle-model experiments, a constant temperature-dependent biospheric CO_2 uptake during different halves of the present century, and in any future warmer world. Such an assumption may lead to underestimates of future atmospheric concentrations of CO_2 and conservative estimates of future warming. However, the real significance of our results, in this regard, can only be gauged by quantifying the impact of reduced tree growth on absolute amounts of carbon sequestered and comparing these with estimates over previous centuries based on earlier tree-ring data. □

Methods

The individual site tree-ring chronologies were produced from multiple increment core samples replicated within and between trees. The individual ring width (TRW) and maximum-latewood-density (MXD) measurement series were corrected for age-related bias by taking residuals from a generalized exponential or "Hugershoff" function of the form $G_t = at^b\exp(-ct)$, where G_t is the biological growth trend, t is time and a, b and c are empirically fitted constants[3]. A simple arithmetic average of the resulting dimensionless indices is computed across each year to form each site chronology. We examined a cross-section of the data looking for systematic misfits of the function in recent years without finding evidence that the results we describe are an artefact of inappropriate standardization.

Before measuring absolute densities, resin and heartwood compounds were extracted with alcohol and water. There was no evidence of heartwood/sapwood bias in the density profiles and no evidence of bias associated with technical difficulties measuring very narrow rings.

The individual MXD and TRW site chronologies were normalized with respect to their mean and standard deviation for the period 1901–40. Within each region, all chronologies were averaged together with a time-dependent weighting equal to the fraction of all possible tree cores that were available for a particular year of each chronology. Each regional mean thus obtained tended to have greater variance during years when few chronologies were available to contribute to the average; this effect was corrected[30] for by scaling by the square root of the effective number (n') of independent samples available in each year, where $n' = n/[1 + (n-1)\bar{r}]$. Here, $\bar{r}$ is the mean intersite correlation between the n chronologies, a measure of the regional-scale common signal. After correction, each regional mean timeseries was normalized with respect to 1881–1940.

Regional mean temperature time series were constructed by averaging together the stated monthly mean temperature anomalies from each 5° by 5° box in which a chronology for that region is located (Fig. 1). The variance of each of these series was also corrected according to the effective number of independent samples that contributed to each year's mean, and was also normalized with respect to 1881–1940. The Northern Hemisphere mean temperature series is made up of all available gridbox data, including land and marine data, north of the Equator.

In the most recent period (1983–92), the regional mean tree-growth timeseries (particularly ALL and NORTH) are spatially biased towards northern Eurasia, due to the earlier development of chronologies in other regions. For comparison, similarly biased temperature time series were constructed by using a time-dependent sampling area defined each year by choosing only those boxes that had MXD and TRW chronology values in them. These biased series were very similar to those temperatures computed from the fixed regional grids (Fig. 1) and do not alter any of the conclusions drawn here.

Received 14 May; accepted 11 November 1997.

1. Schweingruber, F. H. *Tree Rings. Basics and Applications of Dendrochronology* (Kluwer, Dordrecht, 1988).
2. Schweingruber, F. H. & Briffa, K. R. in *Climate Variations and Forcing Mechanisms of the Last 2000 Years* (eds Jones, P. D., Bradley, R. S. & Jouzel, J.) 43–66 (Springer, Berlin, 1996).
3. Bräker, O. Der Alterstrend bei Jahrringdichten und Jahrringbreiten von Nadelhölzern und sein Ausgleich. *Mitt. forstl. Bundesvers Anst Wien* **142,** 75–102 (1981).
4. Briffa, K. R., Jones, P. D., Schweingruber, F. H., Karlén, W. & Shiyatov, S. G. in *Climate Variations and Forcing Mechanisms of the Last 2000 Years* (eds Jones, P. D., Bradley, R. S. & Jouzel, J.) 9–41 (Springer, Berlin, 1996).
5. Cook, E. R., Briffa, K. R., Meko, D. M., Graybill, D. A. & Funkhouser, G. The 'segment-length curse' in long tree-ring chronology development for palaeoclimatic studies. *Holocene* **5,** 229–237 (1995).
6. Schweingruber, F. H., Briffa, K. R. & Nogler, P. A tree-ring densitometric transect from Alaska to Labrador. *Int. J. Biometeorol.* **37,** 151–169 (1993).

7. D'Arrigo, R. D., Jacoby, G. C. & Free, R. M. Tree-ring width and maximum latewood density at the North American tree line: parameters of climate change. *Can. J. Forest Res.* **22,** 1290–1296 (1992).
8. Graybill, D. A. & Shiyatov, S. G. in *Climate Since A. D. 1500* (eds Bradley, R. S. & Jones, P. D.) 393–414 (Routledge, London, 1992).
9. Graumlich, L. J. A 1000-year record of temperature and precipitation in the Sierra Nevada. *Quat. Res.* **39,** 249–255 (1993).
10. Cook, E. R., Briffa, K. R. & Jones, P. D. Spatial regression methods in dendroclimatology: a review and comparison of two techniques. *Int. J. Climatol.* **14,** 379–402 (1994).
11. Jones, P. D. & Briffa, K. R. Global surface air temperature variations during the twentieth century: Part 1, spatial, temporal and seasonal details. *Holocene* **2,** 165–179 (1992).
12. Jacoby, G. C. & D'Arrigo, R. D. Reconstructed Northern Hemisphere annual temperature since 1671 based on high-latitude tree-ring data from North America. *Clim. Change* **14,** 39–49 (1989).
13. Jacoby, G. C. & D'Arrigo, R. D. Tree ring width and density evidence of climatic and potential forest change in Alaska. *Glob. Biogeochem. Cycles* **9,** 227–234 (1995).
14. Briffa, K. R., Jones, P. D. & Hulme, M. Summer moisture variability across Europe, 1892–1991: an analysis based on the Palmer Drought Severity Index. *Int. J. Climatol.* **14,** 475–506 (1994).
15. Nicholls, N. *et al.* in *Climate Change 1995* (eds Houghton, J. T. *et al.*) 133–192 (Cambridge Univ. Press, 1996).
16. Groisman, P. Y., Karl, T. R. & Knight, R. W. Observed impact of snow cover on the heat balance and the rise of continental spring temperatures. *Science* **263,** 198–200 (1994).
17. Hogg, P. H. & Hurdle, P. A. The aspen parkland in western Canada: a dry-climate analogue for the future boreal forest? *Wat. Air Soil Pollut.* **82,** 391–400 (1995).
18. Fleming, R. A. & Volney, J. A. Effects of climate change on insect defoliator population processes in Canada's boreal forest: some plausible scenarios. *Wat. Air Soil Pollut.* **82,** 445–454 (1995).
19. DeLuisi, J. J. *et al.* Northern and middle-latitude ozone profile features and trends observed by SBUV and Umkehr, 1979–1990. *J. Geophys. Res.* **99,** 18901–18908 (1994).
20. Sullivan, J. H. in *Stratospheric Ozone Depletion/UV-B Radiation in the Biosphere* (eds Biggs, R. H. & Joyner, M. E. B.) 67–76 (Springer, Berlin, 1994).
21. Tevini, M. in *Stratospheric Ozone Depletion/UV-B Radiation in the Biosphere* (eds Biggs, R. H. & Joyner, M. E. B.) 37–56 (Springer, Berlin, 1994).
22. Bryson, R. A. & Goodman, B. M. Volcanic activity and climatic changes. *Science* **207,** 1041–1044 (1980).
23. Asaturov, M. L. *et al. Volcanoes, Stratospheric Aerosols and Earth's Climate* (Gidrometeoizdat, Leningrad, 1986) [In Russian].
24. Bradley, R. S. & Jones, P. D. in *Climate Since A.D. 1500* (eds Bradley, R. S. & Jones, P. D.) 606–622 (Routledge, London, 1992).
25. Melillo, J. M., Prentice, I. C., Farquhar, G. D., Schulz, E.-D. & Sala, O. E. in *Climate Change 1995* (eds Houghton, J. T. *et al.*) 444–481 (Cambridge Univ. Press, 1996).
26. Hättenschwiler, S., Schweingruber, F. H. & Körner, C. Tree ring responses to elevated CO_2 and increased N deposition in *Picea Abies*. *Plant Cell Environ.* **19,** 1369–1378 (1996).
27. Wigley, T. M. L. Balancing the carbon budget. Implications for projections of future carbon dioxide concentration changes. *Tellus B* **45,** 409–425 (1993).
28. Craig, S. G. & Holmén, K. J. Uncertainties in future CO_2 projections. *Glob. Biogeochem. Cycles* **9,** 139–152 (1995).
29. Ciais, P., Tans, P. P., Trolier, M., White, J. W. C. & Francey, R. J. A large northern hemisphere terrestrial CO_2 sink indicated by the $^{13}C/^{12}C$ ratio of atmospheric CO_2. *Science* **269,** 1098–1102 (1995).
30. Osborn, T. J., Briffa, K. R. & Jones, P. D. Adjusting variance for sample size in tree-ring chronologies and other regional-mean timeseries. *Dendrochronologia* (in the press).

Acknowledgements. We thank P. Nogler, T. Forster, B. Feiertag and E. Schär, WSLFNP, for densitometry and chronology construction, and G. Jacoby and C. Körner for comments on the manuscript. This work was supported by the Swiss Federal Institute of Forest, Snow and Landscape Research, the Swiss National Science Foundation, the European Community Environment and Climate Programme and the UK NERC.

Correspondence and requests for materials should be addressed to K.R.B. (e-mail: k.briffa@uea.ac.uk).

Evidence for partial melt at the core–mantle boundary north of Tonga from the strong scattering of seismic waves

John E. Vidale* & Michael A. H. Hedlin†

* *Department of Earth and Space Sciences, University of California, Los Angeles, Los Angeles, California 90095-1567, USA*
† *Cecil H. and Ida M. Green Institute of Geophysics and Planetary Physics, University of California, San Diego, La Jolla, California 92093-0225, USA*

Scattered waves that precede the seismic phase PKP (which traverses the Earth's core) have been used to identify and locate small-scale heterogeneity in the Earth's mantle[1–6]. A recent study has demonstrated that the global data set of these precursors is consistent with weak heterogeneity (about 1 per cent r.m.s. velocity variation) distributed throughout the mantle[7]. Here we show, however, that anomalously large PKP precursors from earthquakes in northern Tonga require much stronger heterogeneity (10–15 per cent r.m.s. velocity variation) in a layer about 60 km thick near the core–mantle boundary below Tonga. This region of the core–mantle boundary is also marked by low shear-wave velocities in the lower mantle[8] and is near an area of very low compressional-wave velocity in the lowermost tens of kilometres of the mantle[9], which has been interpreted as evidence for the presence of partial melt[10]. The strength of the scattering that we observe provides strong support for the presence of partial melt in this area, and also suggests that vigorous small-scale convection is taking place at the core–mantle boundary.

The nature of the lowermost mantle remains elusive. As the core–mantle boundary (CMB) is the lower bound on mantle convection, it must underlie at least a thermal boundary layer[11]. However, just above the CMB may also be home to chemical heterogeneity[12]. The lowermost mantle shows two kinds of seismic structure. First, layering in P- and S-wave velocities and anisotropy is seen in the few hundred kilometres above the CMB[13]. Second, weak fine-scale heterogeneity is inferred from scattered waves that precede the seismic phase PKP[1–6]. Until recently, the few per cent amplitudes inferred for these two types of structures were small enough that variations in mineralogy and reasonable temperature differences without melt could provide an explanation[7,11,14]. One or more patches of the CMB, which correlate with large-scale slower than average lower mantle, seem to have greater perturbations. Recent work[9,15] suggests P-wave velocity reductions of ~10% in the lowest

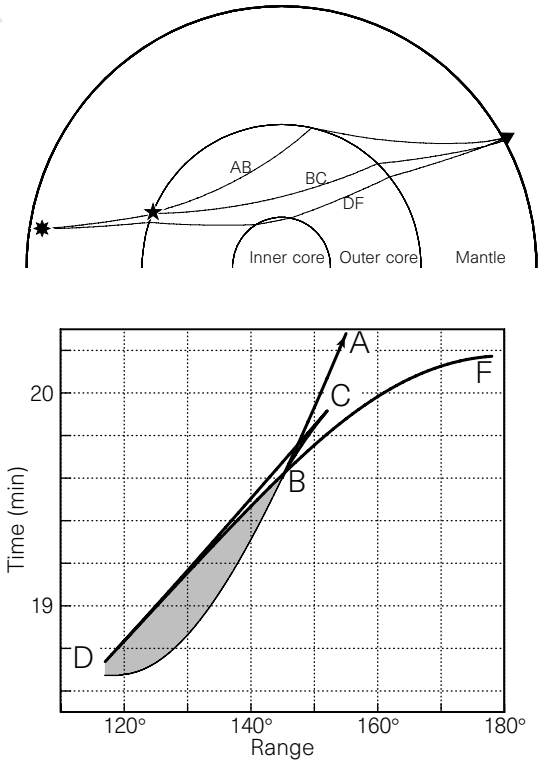

Figure 1 Ray-paths and travel times of PKP phases. A receiver located 140° from an earthquake can detect seismic energy that has passed through the inner core (PKP_{df}) as well as energy deflected from P to the outer core branches PKP_{ab} and PKP_{bc} by a scatterer located at the CMB. Owing to the unusual ray geometries caused by the sharp drop in P-wave velocity at the CMB, this scattered energy can precede PKP_{df}. Although we have depicted near-source scattering at the CMB, scattering at any depth in the mantle at either end of the path can give rise to precursors. The lower panel shows the four branches of PKP from a surface event. In addition to the inner and outer core refracted phases just discussed is PKP_{cd}, the phase that reflects off the inner core. Possible arrival times for the precursors are indicated by the shaded region. In the top panel, the eight-pointed star marks the earthquake, the five-pointed star marks a possible scattering region, and the triangle marks the receiver.